International Symposium
On Turbulence and Shear Flow
Phenomena (TSFP-9)
June 30 - July 3, 2015 *Melbourne, Australia*

Transitional structures and sound emission in a supersonic round jet forced by a pair of helical modes

Daisuke Watanabe
Graduate School of Engineering
Toyama University
3190 Gofuku, Toyama-shi, Toyama 930-8555, Japan
dwata@eng.u-toyama.ac.jp

Hiroshi Maekawa
Graduate School of Informatics and Engineering
The university of electro-communications
1-5-1 Chofugaoka, Chofu-shi, Tokyo 182-8585, Japan
maekawa@mce.uec.ac.jp

ABSTRACT

The three-dimensional compressible Navier-Stokes equations are numerically solved to study the transitional structure and the resultant acoustic emission in a supersonic round jet at high convective Mach numbers. A 5th-order compact upwind algorithm developed by Deng et al. (1996) is used for spatial derivatives and a 4th-order Runge-Kutta scheme for time advancement. The Navier-Stokes characteristic boundary conditions are used in the streamwise and radial directions and periodic boundary conditions in the azimuthal direction. Numerical results for the convective Mach number Mc = 1.00 (M_j=2.0) and Re_{r0}=1000 based on the jet nozzle radius r_0 are presented. Four different cases were investigated. The first case is the jet forced randomly (random case). The other cases are the jet flow forced by the linear unstable modes. These cases are the jet flow forced by a pair of first helical modes(m=±1 case), second helical modes(m=±2 case) and third helical modes(m=±3 case), respectively. Growth of a pair of third helical modes (m=±3) causes the early decay of jet centerline velocity. Furthermore, radiated pressure fluctuations generated by the growth of a pair of third helical modes (m=±3) which have subsonic phase velocity are suppressed compared with turbulent jet.

INTRODUCTION

Compressible jets, which can be found in many applications such as rocket, scramjet, ramjet and turbojet engines, have been of fundamental importance in the study of compressible free shear flows. With new noise regulations, reducing of acoustic noise is the one of key technological challenges facing proposed supersonic commercial aircraft. The numerical investigation of supersonic jets is expected to guide such technological progress on aircraft where the jet exhaust velocity is supersonic. On the other hand, methods have long been sought to find an efficient means for reduction of jet noise using either active or passive turbulence control measures (see Seiner 1992). Progress in this area has been limited by unclear understanding of the physical supersonic jet noise source mechanism. These mechanisms have been extensively studied using round jets. Non-round geometry of the jet exit has been experimentally studied for beneficial noise reduction relative to the round jets. Mach wave emission and shock noise are the dominant acoustic sources of supersonic jet noise. Improperly expanded nozzles produce shock noise that dominates acoustic emission in the jet forward quadrant. Shock noise, however, could be minimized through appropriate design of nozzle geometry. It has been observed experimentally that the acoustic radiation from jets is dominated by Mach waves (see review by Tam 1995). Turbulent structures traveling at supersonic speed within the jet are generally thought to be responsible for Mach waves, and they have been modelled as a combination of linearly unstable modes. Reduction of Mach wave emission represents the most serious challenge to the successful design of a suppressor nozzle. The understanding of jet turbulence and noise emission is very crucial for jet investigations. DNS of supersonic round jet was performed and brought much light to these mechanisms. Freund et al. (2000) simulated a perfectly expanded Mach 1.92 jet at Re_D=2000 and its sound field. Watanabe et al. (2003, 2006) performed linear stability analysis and DNS of a supersonic plane jet. Their results show that the plane jet (M_c =1.17) forced by a pair of oblique modes (the oblique mode is most unstable at high convective Mach numbers) with the subsonic phase speed suppresses the emitted Mach wave intensity. On the other hand, in thigh convective Mach number, the most unstable (first helical mode) modes have the supersonic phase speed in a round jet (Luo et al., 1997, Parras et al., 2010 and Watanabe 2014). The supersonic phase speed of the most unstable mode in a round jet makes the suppression of Mach waves more difficult.

The linear inviscid instability wave model and Lighthill acoustic analogy approach have provided invaluable guidance to the development of the jet noise prediction (see Zorumski 1982). It is generally accepted that the mechanism for Mach wave radiation (Tam et al., 1984) (as well as growth of compressible mixing layers, Morris et al., 1990) is strongly connected with the amplification rate of instability modes and that the instability wave scales with the convective Mach number. The real physical process, however, involves nonlinear interaction of various instability modes in the flow filed. DNS researches of the nonlinear interaction for the supersonic jets in the transition regime are important for understanding of these mechanisms.

We investigate, by means of DNS, the spatially development of high Mach number round jet forced with the unstable/random disturbances. Both the fluid dynamic structures and noise of round jets are studied. In the present study, we focus on the effect of inflow disturbances on the Mach wave emission from the round jet using spatial 3-D DNS. The round jet is of interest, as described above, due to practical importance of supersonic combustion and jet noise generation. The sound fields related to the energy nonlinear evolution of various a pair of linear unstable modes are examined at high convective Mach numbers. In this pair, the effects of growth of a pair of first, second and third helical modes (m=±1, m=±2 and m=±3; m indicates the azimuthal wave number) on the jet sound fields and flow field in a round jet are presented.

NUMERICAL METHODS

In the direct numerical simulation, the non-dimensional equations governing the conservation laws of mass, momentum, and energy for a compressible Newtonian fluid are solved using a fifth-order compact upwind algorithm for conservation form [1] with a time integration 4th-order Runge-Kutta algorithm. The governing equations in cylindrical coordinates are given as follows;

$$\frac{\partial \rho}{\partial t}+\frac{1}{r}\frac{\partial (r\rho u_r)}{\partial r}+\frac{1}{r}\frac{\partial (\rho u_\theta)}{\partial \theta}+\frac{\partial (\rho u_x)}{\partial x}=0, \quad (1)$$

$$\frac{\partial (\rho u_r)}{\partial t}+\frac{1}{r}\frac{\partial (r\rho u_r u_r)}{\partial r}+\frac{1}{r}\frac{\partial (\rho u_r u_\theta)}{\partial \theta}+\frac{\partial (\rho u_r u_x)}{\partial x}-\frac{\rho u_\theta u_\theta}{r}=-\frac{\partial p}{\partial r}+\left[\frac{1}{r}\frac{\partial (r\tau_{rr})}{\partial r}+\frac{1}{r}\frac{\partial \tau_{r\theta}}{\partial \theta}-\frac{\tau_{\theta\theta}}{r}+\frac{\partial \tau_{rx}}{\partial x}\right], \quad (2)$$

$$\frac{\partial (\rho u_\theta)}{\partial t}+\frac{1}{r}\frac{\partial (r\rho u_r u_\theta)}{\partial r}+\frac{1}{r}\frac{\partial (\rho u_\theta u_\theta)}{\partial \theta}+\frac{\partial (\rho u_\theta u_x)}{\partial x}+\frac{\rho u_r u_\theta}{r}=-\frac{1}{r}\frac{\partial p}{\partial \theta}+\left[\frac{1}{r^2}\frac{\partial (r^2\tau_{\theta r})}{\partial r}+\frac{1}{r}\frac{\partial \tau_{\theta\theta}}{\partial \theta}+\frac{\partial \tau_{\theta x}}{\partial x}\right], \quad (3)$$

$$\frac{\partial (\rho u_x)}{\partial t}+\frac{1}{r}\frac{\partial (r\rho u_r u_x)}{\partial r}+\frac{1}{r}\frac{\partial (\rho u_\theta u_x)}{\partial \theta}+\frac{\partial (\rho u_x u_x)}{\partial x}=-\frac{\partial p}{\partial x}+\left[\frac{1}{r}\frac{\partial (r\tau_{xr})}{\partial r}+\frac{1}{r}\frac{\partial \tau_{x\theta}}{\partial \theta}+\frac{\partial \tau_{xx}}{\partial x}\right], \quad (4)$$

$$\frac{\partial Et}{\partial t}+\frac{1}{r}\frac{\partial [r(Et+p)u_r]}{\partial r}+\frac{1}{r}\frac{\partial [(Et+p)u_\theta]}{\partial \theta}+\frac{\partial [(Et+p)u_x]}{\partial x}=\frac{1}{r}\frac{\partial (ru_i\tau_{ir})}{\partial r}+\frac{1}{r}\frac{\partial (u_i\tau_{i\theta})}{\partial \theta}+\frac{\partial (u_i\tau_{ix})}{\partial x}+\frac{1}{r}\frac{\partial}{\partial r}\left(\kappa r\frac{\partial T}{\partial r}\right)+\frac{1}{r^2}\frac{\partial}{\partial \theta}\left(\kappa\frac{\partial T}{\partial \theta}\right)+\frac{\partial}{\partial x}\left(\kappa\frac{\partial T}{\partial x}\right), \quad (5)$$

where

$$E_t=\frac{p}{(\gamma-1)}+\frac{\rho u_x u_x}{2}+\frac{\rho u_r u_r}{2}\frac{\rho u_\theta u_\theta}{2}, \quad (6)$$

$$\tau_{xx}=\frac{\mu}{\mathrm{Re}}\left\{\left(2\frac{\partial u_x}{\partial z}\right)-\frac{2}{3}\left[\frac{1}{r}\frac{\partial (ru_r)}{\partial r}+\frac{1}{r}\frac{\partial u_\theta}{\partial \theta}+\frac{\partial u_x}{\partial x}\right]\right\},$$

$$\tau_{rr}=\frac{\mu}{\mathrm{Re}}\left\{\left(2\frac{\partial u_r}{\partial r}\right)-\frac{2}{3}\left[\frac{1}{r}\frac{\partial (ru_r)}{\partial r}+\frac{1}{r}\frac{\partial u_\theta}{\partial \theta}+\frac{\partial u_x}{\partial x}\right]\right\},$$

$$\tau_{\theta\theta}=\frac{\mu}{\mathrm{Re}}\left\{\left[2\left(\frac{1}{r}\frac{\partial u_\theta}{\partial \theta}+\frac{u_r}{r}\right)\right]-\frac{2}{3}\left[\frac{1}{r}\frac{\partial (ru_r)}{\partial r}+\frac{1}{r}\frac{\partial u_\theta}{\partial \theta}+\frac{\partial u_x}{\partial x}\right]\right\},$$

$$\tau_{xr}=\tau_{rx}=\frac{\mu}{\mathrm{Re}}\left(\frac{\partial u_r}{\partial x}+\frac{\partial u_x}{\partial r}\right),$$

$$\tau_{r\theta}=\tau_{\theta r}=\frac{\mu}{\mathrm{Re}}\left[r\frac{\partial}{\partial r}\left(\frac{u_\theta}{r}\right)+\frac{1}{r}\frac{\partial u_r}{\partial \theta}\right],$$

$$\tau_{\theta x}=\tau_{x\theta}=\frac{\mu}{\mathrm{Re}}\left(\frac{1}{r}\frac{\partial u_x}{\partial \theta}+\frac{\partial u_\theta}{\partial x}\right), \quad (7)$$

$$\kappa = -\frac{\mu}{(\gamma-1)M^2 RePr}, \tag{8}$$

$$T = \frac{\gamma M^2 p}{\rho}, \tag{9}$$

$$\mu = T^{2/3}, \tag{10}$$

where $M = U_j / c_\infty$ and c_∞ is the speed of sound at the ambient fluid. The all variables, in all the following discussions, are non-dimensionalized by the characteristic physical scales such as U_j, ρ_∞, T_∞ and the jet nozzle radius of r_0 where the subscripts j and ∞ indicate the jet centerline and the ambient fluid, respectively. The Reynolds number is

$$Re = \frac{U_j r_0}{\mu_\infty}. \tag{11}$$

The flow field of a jet issuing from circular nozzle into an ambient fluid can be divided into a potential core region, a transition region, and a fully developed region. The "top-hat" jet profile belongs to the potential core region with a thin but finite shear layer. We employed the mean velocity profile $U(r)$ given by

$$U(r) = \frac{U_j}{2}\left\{1 - \tanh\left[\frac{12.5}{4}\left(\frac{r}{r_0} - \frac{r_0}{r}\right)\right]\right\}. \tag{12}$$

The mean temperature $\overline{T}(r)$ was calculated with the Crocco-Busemann relation for unity Prandtl number;

$$\overline{T}(r) = M_\infty^2 \frac{\gamma-1}{2}\frac{(U_j U(r) - U(r)^2)}{U_j} + \frac{T_\infty (U_j - U(r))}{U_j} + \frac{T_j U(r)}{U_j}, \tag{13}$$

where γ is the ratio of specific heats. $M_\infty = U_j / c_\infty$ and c_∞ is the speed of sound at the quiescent stream. The jet centerline Mach number $M_j = U_j / c_j$ is obtained from the relation $M_j = M_\infty c_\infty / c_j$. The jet was heated with exit temperature ratio $T_j / T_\infty = 1.12$. This ratio was used for the simulation of a perfectly expanded Mach 1.92 jet (Watanabe et al., 2002). A jet convective Mach number M_c may be defined by

$$M_c = \frac{M_j \sqrt{T_j / T_\infty}}{1 + \sqrt{T_j / T_\infty}}. \tag{14}$$

By using equation (14), the convective Mach number for the present study is M_c = 0.97 (M_j= 1.89).

For 3-D spatial DNS, after a grid-convergence analysis, the computational mesh was $N_x \times N_r \times N_\theta$ = 801×150×128. Mesh points were clustered toward the jet shear layer in the normal direction and downstream streamwise locations near the end of the potential core. NSCBC (the Navier-Stokes Characteristic Boundary Conditions, Poinsot et. al., 1992) were implemented in the treatment of the boundaries at the in/outflow and far normal regions. Periodic boundary conditions were implemented in the azimuthal direction. Outflow boundaries were located at x=35r_0 in the streamwise direction and at r = 20r_0. For a pair of helical modes case (m=±1, m=±2 and m=±3 case), the inlet disturbance vector $\tilde{\mathbf{d}}_{in} = (\tilde{\rho}_{in}, \tilde{u}_{xin}, \tilde{u}_{rin}, \tilde{u}_{\theta in}, \tilde{p}_{in})$ can be written as

$$\tilde{\mathbf{d}}_{in} = \sum_m A_m \hat{d}_{m.}(r) \exp\{\mathrm{i}[m\theta - (2\pi St)t]\}, \tag{15}$$

where $\hat{d}_m$ is the eigenfunction of corresponding instability mode calculated by linear stability analysis. m and St indicate the corresponding azimuthal wave number and nondimensional frequency. The amplitude of each mode is 2% of the jet and the Strouhal numbers are set to be St=0.1 closely corresponding to the maximum growth rate. On the other hand, the magnitude of the forced streamwise velocity disturbance is chosen to be 10% of the jet centerline velocity for the random case.

RESULTS

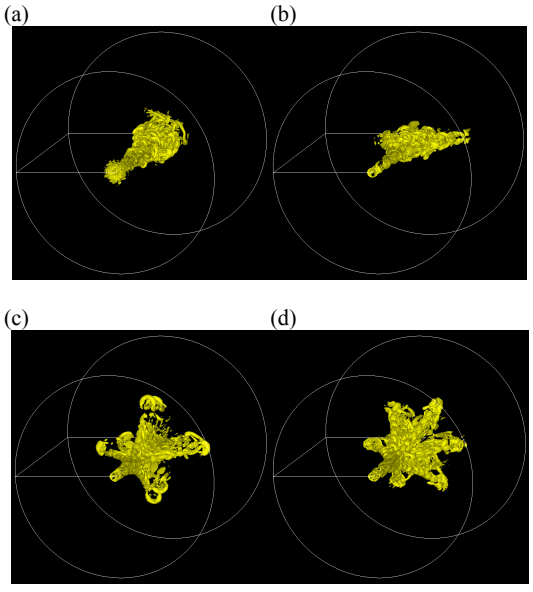

Figure 1. Second invariant Q structure (iso-surfaces of Q=0.01) for a) random case, b) m=±1 case, c) m=±2 case and d) m=±3 case.

Figure 1 shows the vortex structures visualized with iso-surfaces of the second invariant Q of the velocity

gradient tensor. Typical vortex structures appear in the jet due to the growth of each inlet disturbance. In the random case, the vortex structures spread almost in all azimuthal directions (the cross-section view at the downstream location shows almost a circle shape from the jet center). In the m=±1 case, m=±2 case and m=±3 case, the vortex structures extend radially in the two, fore, six distinct azimuthal directions from the jet center line, respectively. In these cases, the vortex structures extend far away as compared with the random case. These characteristic expansions of vortex structures affect the jet velocity. Figure 2 shows the contour plots of instantaneous streamwise velocity at $x=32r_0$ where $y=r/r_0 \cos\theta$ and $z=r/r_0 \sin\theta$. In these figures, the same characteristic distributions as the vortex structures are also seen in the jet stream wise velocity.

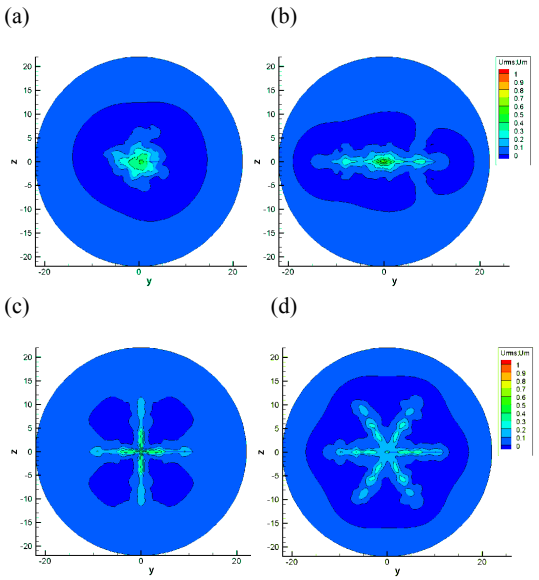

Figure 2. The contour plots of instantaneous streamwise velocity for a) randomcase, a pair of b) first helical modes case (m=±1), c) second helical modes case (m=±2) and d) third helical modes case (m=±3) at $x=32r_0$.

Figures 3(a), (b), (c) and (d) show the downstream evolution of mean streamwise velocity for random case, m=±1 case, m=±2 case and m=±3 case, respectively. In the random case, the contour plots of mean streamwise velocity spread gradually towards the downstream (Figure 3a). On the otherhand, in the m=±1 case, m=±2 case and m=±3 case, growth of a pair of helical modes leads to sooner shear layers expansions around the end of jet potential region. Figure 3(b), (c) and (d) indicate that the shear layers spread rapidly around $x=22r_0$, $x=15r_0$, $x=20r_0$, for m=±1 case, m=±2 case and m=±3 case, respectively. Around these points correspond with the point that characteristic expansions of vortex structures appear.

The centerline streamwise velocity shown in figure 4 clearly indicates the location where the potential core closes. The inflow disturbance also influences on the jet center line velocity distribution, as shown in Figure 4. In the m=±3 case, the jet center line velocity decreases sooner to u_c=0.2 at the downstream location of $x=35r_0$, though the jet center line velocity of the random case decreases to u_c=0.4 at the same location.

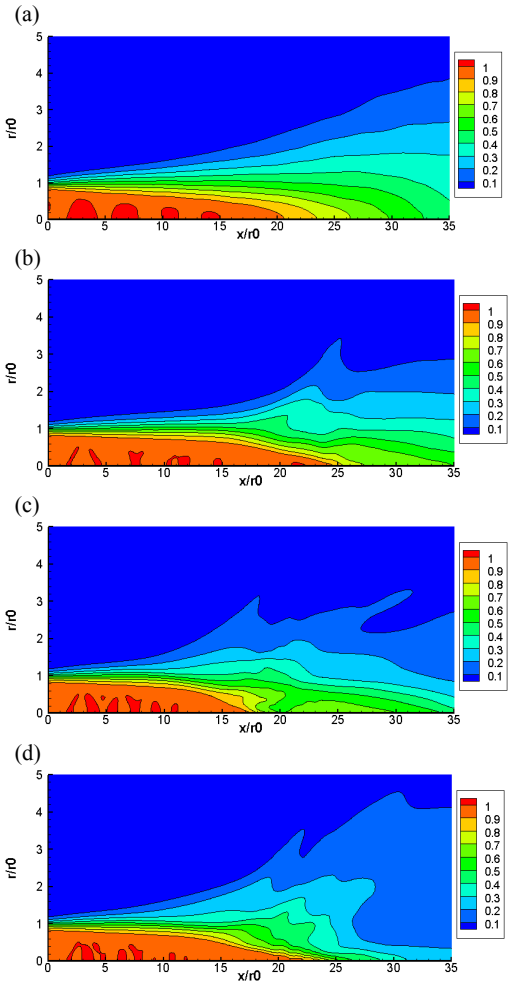

Figure 3. Downstream evolution of mean streamwise velocity (contour plots); a) random case, a pair of b) first helical modes case (m=±1), c) second helical modes case (m=±2) and d) third helical modes case (m=±3) at $x=32r_0$.

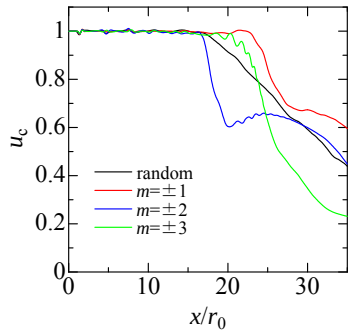

Figure 4. Mean jet centerline velocity.

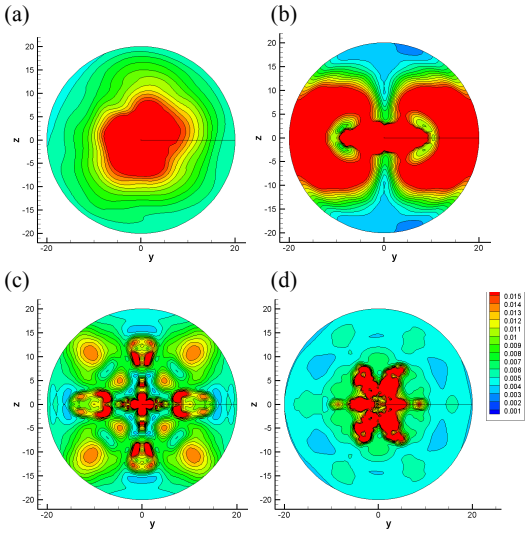

Figure 5. RMS of overall fluctuating pressure for a) randomcase, a pair of b) first helical modes case (m=±1), c) second helical modes case (m=±2) and d) third helical modes case (m=±3) at $x=32r_0$.

Figures 5 indicates RMS of overall fluctuating pressure for the each case at $x=32r_0$. In the $m=\pm1$ case, $m=\pm2$ case and $m=\pm3$ case, the distributions of pressure fluctuation magnitudes show the different geometric patterns. These patterns are caused by interfering between the pair of helical modes with the same frequency propagating mutually but in the opposite directions. Note that, with the increase of the azimuthal wave number m, the pressure fluctuation magnitudes become smaller at the jet far field. In the $m=\pm3$ case, radiated pressure fluctuations are especially smaller compared with the other cases.

In order to find the reason of the pressure fluctuations in the jet mentioned the above, the linear stability analyses are carried out. Turbulent structures traveling at supersonic speed in the jet are generally thought to be responsible for Mach waves (see Papamoschou, 1997, Morris 2010 and Kearney-Fischer et al., 2011). Figure 6 shows the Reynolds number dependence of the maximum linear growthrate ω_i and the phase velocity c_r corresponds with the maximum growth rate of the each helical mode. With the increase of the azimuthal wave number m, the maximum linear growth rate and phase velocity becomes smaller over the Reynolds number range shown in the figure. For $m=3$ at $Re=1000$, the phase velocity is lower than acoustic velocity of the ambient fluid c_∞, and c_r/c_∞ remain near unity at high Reynolds number. This result suggests that the third helical mode may much less contribute to radiation of Mach waves. As figures 2 and 3 show, the third helical mode is a good candidate to eliminate the acoustic waves in the round jet. DNS of the jet effectively forced by the third helical mode will be performed to achieve the Mach wave elimination at high Mach number.

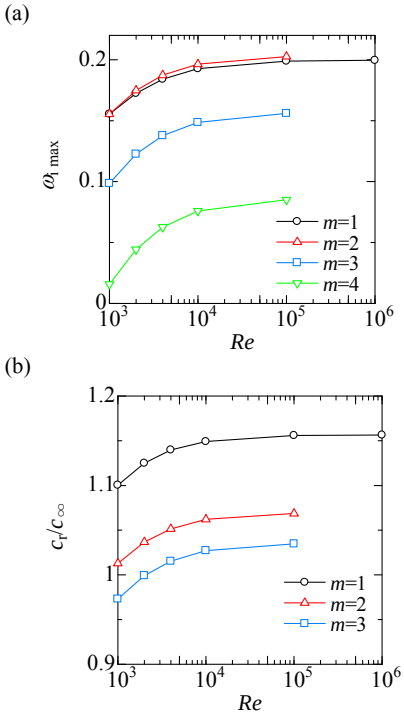

Figure 6. Reynolds number dependence of a) maximum linear groth rate and b) phase velocity of the helical mode at maximum growth rate.

CONCLUSIONS

Spatial DNS of a supersonic round jet for $Mc=2.0$ has been performed. The numerical results provide new physical insights into jet expansion and noise generation in a round jet. Upstream disturbance conditions play an important role for the evolution of the downstream structure, such as development of shear layers and transition process in a jet. Growth of a pair of helical modes is responsible for the characteristic expansions of vortex structure and streamwise velocity in a round jet. Especially growth of a pair of third helical modes ($m=\pm3$) causes the early decay of jet centerline velocity. Furthermore, radiated pressure fluctuations generated by the growth of a pair of third helical modes ($m=\pm3$) which have subsonic phase velocity are suppressed compared with turbulent jet.

ACKNOWLEDGMENTS

This work was supported by JSPS KAKENHI Grant Number 24560189 and 15K05787. Some of the simulations were executed at the Information Technology Center of the University of Tokyo.

REFERENCES

Deng, X., Maekawa, H. and Shen, C., A Class of High Order Dissipative Compact Schemes, AIAA Paper, No. 96-1972 (1996).

Freund J B, Lele S K and Moin P., Numerical Simulation of a Mach 1.92 Turbulent Jet and Its Sound Field, AIAA J. Vol.38, No.11 (2000), pp.2023-2031.

Kearney-Fischer, M.; Kim, J. -H.; Samimy, M., A study of Mach wave radiation using active control, J. Fluid Mech. Vol.681 (2011), pp.261-292.

Luo K H and Sandham N D, Instability of vortical and acoustic modes in supersonic round jets, Phys. Fluids Vol.9, No.4 (1997), pp. 1003-1013.

McLaughlin, D. K., Morrison, G. L. and Troutt, T. R. Reynolds Number Dependence in Supersonic Jet Noise, AIAA J. Vol.15(1977), pp.526-532.

Morris P. J., Gridharan M. G. and Lilley G. M., On the Turbulent Mixing of Compressible Free Shear Layers Proceeding of the Royal Society of London, Series A 431 (1990), pp.219-243.

Morris P. J., The instability of high speed jets, International Journal of Aeroacoustics, Vol. 9, Nos. 1–2, 2010, pp. 1–50.

Papamoschou, D., Mach wave elimination in supersonic jets, AIAA J. Vol.35, No.10 (1997), pp.1604-1611.

Parras, L.,Le Dizes, S., Temporal instability modes of supersonic round jets, J. Fluid Mech. Vol.662 (2010), pp.173-196.

Poinsot T J and Lele S K Boundary Conditions for Direct Simulations of Compressible Viscous Flows J. Comput. Phsy. Vol.101 (1992), pp.104-129.

Seiner J. M., Fluid Dynamics and Noise Emission Associated with Supersonic Jets Studies in Turb (1992), pp.297-323.

Tam C K W and Burton D E Sound Generated by Instability Waves of Supersonic Flows, Part2. Axisymmetric Jets, J. Fluid Mech. Vol.138 (1984), pp.273-295.

Tam C K W Supersonic Jet Noise Annu. Rev. of Fluid Mech. Vol.27 (1995), pp.17-43.

Watanabe D and Maekawa H. Transition of Supersonic Plane Jet due to Symmetric/Antisymmetric Unstable Modes. Journal of Turbulence, Vol.3, No.1 (2002), p.047.

Watanabe D, Maekawa H and Matsuo Y, Effects of Unstable Oblique Modes on the Acoustic Filed in a Supersonic Plane Turbulent Jet, Trans. of the JSME Vol.73, No.724 B (2006), pp.2878-2885 (in Japanese).

Watanabe D and Maekawa H, The effect of upstream disturbance on the angle of sound emission in a supersonic round jet, Journal of Fluid Science and Technology, Vol. 9, No. 3, JFST0054, pp.1-12.

Zorumski W E Aircraft Noise Prediction Program Theoretical Manual NASA TM-83199 (1982).